PHYSICAL REVIEW B **82**, 060503(R) (2010)

Tunable phase diagram and vortex pinning in a superconductor-ferromagnet bilayer

L. Y. Zhu,[1] Marta Z. Cieplak,[1,2] and C. L. Chien[1]
[1]*Department of Physics and Astronomy, The Johns Hopkins University, Baltimore, Maryland 21218, USA*
[2]*Institute of Physics, Polish Academy of Sciences, 02 668 Warsaw, Poland*
(Received 12 July 2010; published 5 August 2010)

We have observed the evolution of phase diagram and vortex pinning using a single ferromagnet/superconductor bilayer of $[Co/Pt]_8/Nb$ through a special demagnetization procedure. It induces a continuous and reversible change in the domain width with equal positive/negative domains enabling the observation of the predicted tunable phase diagram. The tunable domain pattern also systematically affects vortex pinning. We have determined the dependence of the activation energy of vortex pinning on domain width, temperature, and magnetic field.

DOI: 10.1103/PhysRevB.82.060503 PACS number(s): 74.78.Fk, 74.25.Dw, 74.25.Ha, 74.25.Wx

Superconducting(S)/ferromagnetic(F) bilayers (SFBs) have been important model systems to study the strong and intricate interplay between superconductivity and magnetism, two long-range orders that are mutually exclusive in the bulk.[1–3] In an SFB, the stray fields from the F layer due to magnetic domains interact with the Cooper pairs in the S layer via the long-range (orbital) interaction. In SFBs, the F layers with perpendicular magnetic anisotropy (PMA) have unique attributes compared to those with in-plane anisotropy. The stray magnetic field that emanates from a magnetic domain penetrating into the S layer has a well-defined direction and can be systematically altered by an external magnetic field.

Both the nucleation of the superconducting order parameter (OP) and the pinning of vortices[1–3] are strongly affected by stray fields. Since superconductivity nucleates in regions where the local fields are minimal,[2] stray field has a profound effect as manifested in the phase diagram consisting of $T_c(H)$ lines, which are the field dependence of the superconducting critical temperature T_c. Some aspects of the theoretical predictions[4] of the reentrant phenomena have been observed experimentally.[5,6] The strong dependence due to magnetic stripe domain width has also been predicted[7] but not yet verified experimentally. Such studies would require a series of SFBs each with an identical S layer and a specific domain pattern in the F layer with PMA with *equal* amount of positive/negative domains and that domain width can be continuously tuned. A magnetic field was previously[6] used to partially switch the multilayer $[Co/Pt]_n$ to create domain patterns with *unequal* amount of +/− domains with unequal domain width. In contrast to theoretically predicted *symmetric* phase diagram, the observed phase diagram is distinctively *asymmetrical* with respect to $H=0$. Such partially switched system is also susceptible to magnetic field during the determination of the phase diagram.

Below T_c, the magnetic textures also create pinning potentials for vortices.[1–3] Experiments, realized mostly in ordered arrays of magnetic nanodots, have uncovered many novel effects, including the commensurability between the vortex lattice and the underlying dot array, vortex channeling, and other dynamic effects.[3] In comparison, fewer studies employ planar SFBs, which offer the prospects of reversible manipulation of the domain pattern. One notable example is SFBs with regular stripe domains, which may be aligned to produce anisotropic vortex pinning.[8,9] Theories predict that pinning should be enhanced in SFBs,[10] a prospect claimed by some experiments[2,8,11] but contradicted by others.[12] A comprehensive picture remains lacking.

In this work we study these phenomena in a single planar SFB consisting of Nb as the S layer and Co/Pt multilayer with PMA as the F layer. It has not been feasible to fabricate a series of SFBs with varying domains in the F layer with equal positive/negative domains and identical superconducting properties in the S layer. Instead, we use a single sample and tune the domain width L by a unique demagnetization procedure, with which the specific stripe domain pattern with zero magnetization can be reversibly defined and erased, resulting in tuning the phase diagram as predicted theoretically.[7] Furthermore, we have also studied the influence of L on the vortex pinning behavior. We have determined the dependence of vortex activation energy on L, T, and H, and provided a comprehensive picture of pinning in the SFB with randomly oriented stripe domain pattern.

The multilayer $Pt(10)/[Co(0.6)/Pt(0.3)]_8/Si(10)/Nb(20)/Si(10)$, with thickness denoted in nanometers, was grown by sputtering at room temperature on a Si substrate. The central Si(10) layer has been inserted to ensure the absence of proximity effects between $[Co/Pt]_8$ and Nb. In this work, the magnetic field, denoted as H, has been applied perpendicular to the film plane. The $[Co/Pt]_8$ multilayer shows a square hysteresis loop with a coercive field of $H_C \approx 750$ Oe at 10 K as shown in Fig. 1(a). The remnant state (denoted as sF) has a single domain with a saturated magnetization M_S. Using ac demagnetization, the F layer can be made unmagnetized with $M=0$ at $H=0$, where $[Co/Pt]_8$ breaks into equal amount of up and down stripe domains with equal domain width. Upon increasing H along the initial (red) curve, M remains very small until H approaches that of $H_C \approx 750$ Oe. In the field range of $|H| \leq 400$ Oe, the magnetic domains remain essentially unchanged, and the external field simply alters the stray field entering the S layer above a magnetic domain.

Previously demagnetization method with either perpendicular or in-plane field has been used to create different domain patterns.[13,14] Unique to this work is the use of an angle-dependent demagnetizing method, in which an ac magnetic field of decreasing magnitude is applied at an angle θ with respect to the film plane as schematically shown in the inset of Fig. 1(i). Magnetic force microscopy (MFM) images [Figs. 1(c)–1(h)] reveal meandering stripe domains with

 ©2010 The American Physical Society

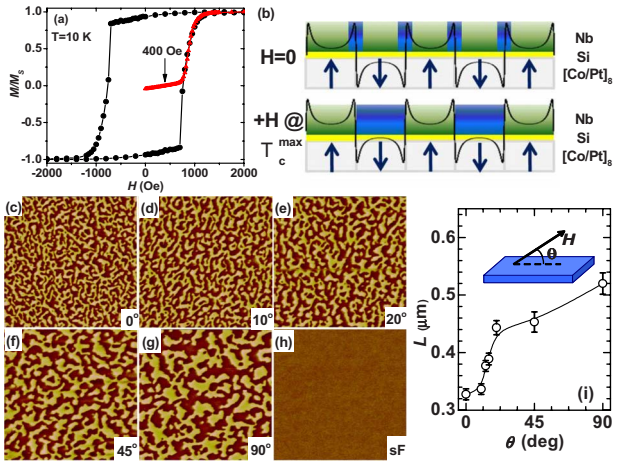

FIG. 1. (Color online) (a) Hysteresis loop at 10 K of $[Co(0.6)/Pt(0.3)]_8$ in a perpendicular field H with the initial curve shown in red, (b) schematics of stray field in Nb due to stripe domains in $[Co(0.6)/Pt(0.3)]_8$. [(c)–(h)] MFM images (10×10 μm^2) at 300 K after demagnetization at angle θ=0°, 10°, 20°, 45°, 90°, and sF, respectively, with the resultant average domain half period L shown in (i).

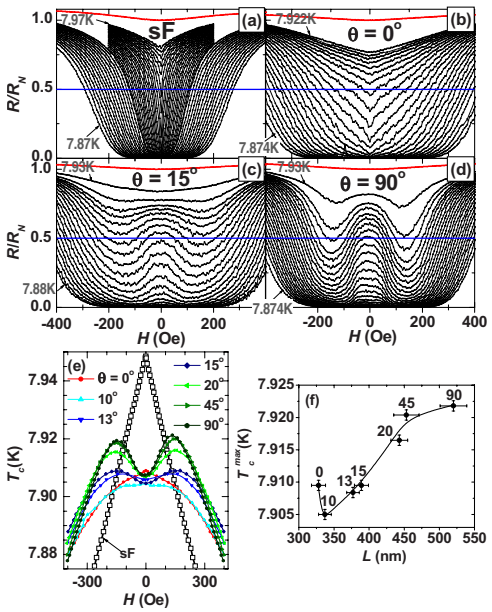

FIG. 2. (Color online) Resistance R (normalized to R_N, the value at 10 K shown in red) versus H in increments of 2–3 mK for states of (a) saturated sF and demagnetized at (b) θ=0°, (c) 15°, and (d) 90°. (e) Values of T_c at R/R_N=0.5 for different θ and (f) the maximal T_c as a function of domain half period L in (e).

equal amounts of positive and negative domains but the average domain width increases monotonically with increasing θ. The meandering stripes in Co/Pt multilayer minimize magnetostatic energy. A two-dimensional (2D) Fourier analysis of the MFM images gives a Gaussian distribution with a mean domain period $2L$ and a standard deviation ΔL. The domain size $L(\theta)$ increases from 328 nm at θ=0° to 520 nm at θ=90° with a standard deviation ΔL of less than 8% [Fig. 1(i)]. The $L(\theta)$ dependence for ferromagnets with PMA can be qualitatively understood as follows. While the magnetic moment is out of plane in the uniform domain area, there is an in-plane component for the magnetic moments within the domain walls. Demagnetizing at a smaller θ tends to align the spins in plane, create more domain walls, hence reducing the domain width. This demagnetizing technique allows the realization of a wide range of domain width $L(\theta)$ using a *single* sample.

The electrical resistance R of the SFB, has been measured on sample 2 mm$\times$5 mm with four contact pads along the long direction and 2 mm between the voltage leads. After each field processing at different θ as well as that in the sF state, R has been measured in a perpendicular magnetic field H at temperature just below T_c in increments of 2–3 mK. As shown in Figs. 2(a)–2(d), while R (normalized to R_N, the normal-state value at 10 K) increases with increasing H and T, the field dependence for different θ is markedly different. The value of R shows one sharp minimum at H=0 for the sF state. The minimum broadens for θ=0°, evolves into two shallow minima at about $\pm$150 Oe for $\theta\approx$15°, and finally becomes two deep minima for $\theta\approx$90°. Defining R/R_N=0.5 as the representative temperature for superconductivity, the values of $T_c(H)$ can be extracted from Figs. 2(a)–2(d). As shown in Fig. 2(e), $T_c(H)$ is linear in H for the sF state, which is single domain and without stray field. Using this result and the coherence length in the dirty limit,[15] $\xi(T)=\xi(0)/(1-T/T_{c0})^{1/2}$, and the upper critical field $H_{c2}(T)=\Phi_0/2\pi\xi^2(T)$, where Φ_0=20.68 G μm^2 is the flux quantum, we obtained T_{c0}=7.95 K and $\xi(0)\approx$12.0 nm.

As shown in Fig. 2(e), $T_c(H)$ is nonlinear for the states processed at θ. Although $T_c(H)$ has a single maximum at H=0 for small θ, it changes to bimodal at large θ with two maxima T_c^{max} at $H\approx\pm$150 Oe, revealing the reentrant phenomenon.[6] The physical origin of the bimodal $T_c(H)$ with T_c^{max} is schematically depicted in Fig. 1(b). The local field is $H_{loc}=H+b_z$, a sum of external field H and stray field b_z with the same direction as that of the domain. At H=0, $H_{loc}=b_z$ with the same magnitude but opposite direction for the up and the down domains. Superconductivity nucleates near the domain-wall regions [blue areas in Fig. 1(b)]. The external field $+H$ applied perpendicular to the plane increases (decreases) the stray field in the up (down) domain. At T_c^{max}, H_{loc}=0 when H compensates the stray field and superconductivity is induced above the oppositely oriented magnetic domains.

The highest T_{c0}=7.95 K occurs at H=0 in the sF state which has effectively infinite L, whereas T_c is suppressed in all other cases [Fig. 2(e)]. As shown in Fig. 2(f), there are two distinct behaviors for $T_c(H)$. For small θ ($L\leq$337 nm), $T_c(H)$ shows one maximum $T_c(0)$ at H=0, whose values decreases with increasing L. For larger θ ($L>$337 nm), $T_c(H)$ is bimodal with two maxima at T_c^{max}, whose values increase with L and appear to saturate at large L. The demarcation point in Fig. 2(f) is at T_c=7.905 K with L=337 nm, corresponding to 2.12ξ, which is close to 2ξ. This key result affirms that $L\approx2\xi$, i.e., the half period L is close to that of the OP.

The OP nucleation in the SFB with periodic stripe domains has been considered theoretically[7] in the context of local field $H_{loc}=H+b_z$. The phase boundary $T_c(H)$ has been

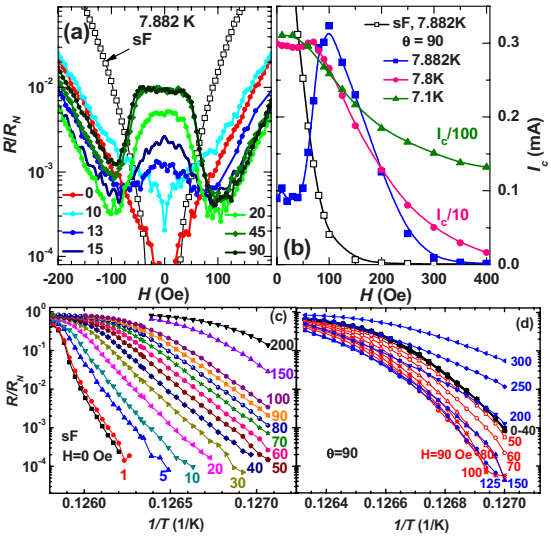

FIG. 3. (Color online) (a) R/R_N versus H at 7.882 K for sF state and various θ. (b) Critical current I_c versus H for sF state at 7.882 K (open squares), and for $\theta=90°$, I_c at 7.882 K (blue), $I_c/10$ at 7.8 K (pink), and $I_c/100$ at 7.1 K (green). (c) R/R_N versus $1/T$ for sF state at labeled magnetic fields $H=0-200$ Oe, and for (d) $\theta=90°$, 0–40 Oe (black), 50–100 Oe (red), and 125–300 Oe (blue).

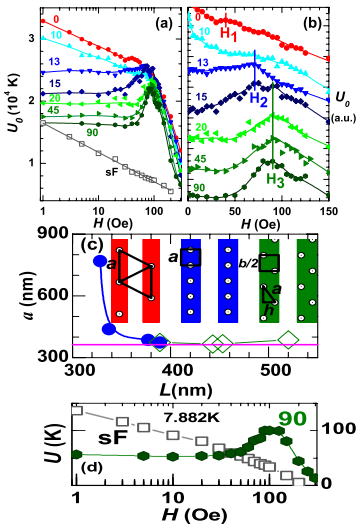

FIG. 4. (Color online) (a) Activation energy U_0 at 0 K versus (a) $\ln H$, (b) H (shifted vertically for clarity) showing peaks at H_1, H_2, and H_3 for sF and different θ, (c) vortex separation a vs L and the schematic vortex structures, for $\theta=0°$ (red), $\theta=15°$ at H_2 (blue), and $\theta=15°$ at H_3 (green); the horizontal line is that for Abrikosov lattice, (d) activation energy $U(H)$ at 7.882 K for sF and $\theta=90°$.

found to depend on the relative size of L and ξ. At $L \ll \xi$, the OP extends over several domains so that the spatial variation in the stray field is averaged out resulting in a single T_c maximum at $H=0$ as we have experimentally realized in states with $L \leq 337$ nm. We note $L \approx 2\xi$ in our case and not $L \ll \xi$. At intermediate L, reentrant $T_c(H)$ line appears with two maxima at $H \approx b_z$, as we have observed in states with $L > 337$ nm. Theory also considers the case for very large $L \gg \xi$, where $T_c(H)$ remains bimodal but with a cusp at $H=0$ in the $T_c(H)$ line. The largest L of about 520 nm may not be sufficiently large to be in this limit. Previously features of reentrant phase diagram have been observed in isolation. We have been able to observe its *continuous* evolution because of our unique sample.

We next turn to the vortex pinning in the tunable SFB. In Fig. 3(a), we show the H dependence of low R at $R/R_N \sim 10^{-2}-10^{-3}$ measured at a lower temperature of 7.882 K ($T/T_{c0}=0.99$). This variation in resistance is the result of the activation of pinned vortices.[16–18] For all angles $\theta > 13°$ we see two minima in R/R_N located symmetrically at about ± 100 Oe with a maximum at $H=0$, which develops into a plateau for $\theta=45°$ and 90°. In Fig. 3(b) we show the critical current $I_c(H)$, defined by the criterion of voltage exceeding 10^{-6} V over 2 mm between the voltage leads, extracted from the I-V characteristics measured at 7.882 K. For the sF state (open squares), $I_c(H)$ decreases sharply and monotonically with H, whereas that of the state with $\theta=90°$ shows a peak at $H \approx 100$ Oe. The presence of domains enhances I_c at 100 Oe, but strongly suppresses I_c for $H \leq 50$ Oe, each by about an order of magnitude. At lower T (at $T/T_{c0}=0.98$ and 0.89), the magnitude of I_c is much larger. But as also shown in Fig. 3(b), I_c reaches saturation as H approaches zero.

To understand this pinning behavior we examine R as a function of $1/T$ as shown in Figs. 3(c) and 3(d). At sufficiently low T all curves become linear, exhibiting a clear Arrhenius behavior. In the case of the sF state [Fig. 3(c)] the |slope| of the linear dependence decreases monotonically with increasing H, indicating a continuous decrease in the flux activation energy U. However, the results for the state with $\theta=90°$ are very different [Fig. 3(d)]. The data for $0 \leq H \leq 40$ Oe are nearly indistinguishable from each other. The |slope| increases with increasing H for $50 \leq H \leq 100$ Oe, above which the |slope| decreases. To extract the activation energy U we follow the previous analysis of the flux activation regime[18] and fit the linear portions on the Arrhenius plots by the dependence of $\ln(R/R_N) = -U_0(H)/(k_B T) + K(H)$. The activation energy in general is $U(T,H) = U_0(H) - K(H)T$, where $U_0(H)$ is the zero-temperature activation energy and $K(H)$ is the coefficient in the linear T correction. Since U vanishes at T_c, it follows that $K(H) = U_0(H)/T_c(H)$. This is indeed the case as all the data falls on a straight line of $U_0(H)/T_c(H)$ vs $K(H)$. Thus, U has the form of $U(T,H) = U_0(H)[1 - T/T_c(H)]$.

In Fig. 4(a), $U_0(H)$, the slope of $\ln(R/R_N)$ vs $1/T$, is shown for various states of the F layer. In the sF state, $U_0(H)$ varies as $\ln H$, which has been reported in epitaxial 2 nm Nb film[18] and attributed to a distribution of pinning strengths, and the preferential "filling" of the strongest pinning sites.[19,20] The U_0 in our 20-nm-thick Nb film is about an order of magnitude larger than that for 2-nm-thick Nb,[18] consistent with pinning in the 2D limit, where U_0 is proportional to the film thickness.

The zero-temperature activation energy U_0 is enhanced by the presence of domains most prominent at $H \leq 40$ Oe. As shown in Fig. 4(a), the enhancement over that of sF is the largest for $\theta=0°$, which also retains partly the $\ln H$ dependence. With increasing θ, U_0 gradually reduces and becomes H independent, which we will comment later. At intermediate H ($40 \leq H \leq 150$ Oe), U_0 takes the form of peaks. At

$H \geq 150$ Oe, U_0 rapidly reduces for all θ, and approaches that of the sF state, when the high vortex density exceeds that of domain-induced pinning centers. In Fig. 4(b), we show U_0 in the intermediate H region on a linear scale and vertically shifted for clarity. One observes peaks at $H_1 \approx 40$ Oe for $\theta=0°$, at $H_2 \approx 70$ Oe for $\theta=10°$, 13°, 15°, and at $H_3 \approx 90$ Oe for $\theta \geq 15°$. Both H_2 and H_3 are present for $\theta=15°$. For $\theta \geq 20°$ only H_3 peak remains.

The peaks in U_0 indicate enhanced pinning when the vortex lattice becomes commensurate with the pinning potential created by the domain pattern. The first matching field H, a condition when a single flux quantum is pinned by each pinning center, corresponds to the average area per vortex $A=\Phi_0/H$.[3] In SFBs with stripe domains, since negative domains are antipinning, vortices exist only in half of the area, $A_n/2=\Phi_0/2H_n$, equal to 2.6×10^{-9} cm^2, 1.5×10^{-9} cm^2, and 1.1×10^{-9} cm^2, for H_1, H_2, and H_3, respectively. Although the disorder in SFB would limit the matching areas, leading to broadening and/or shifting of the matching fields, we nevertheless gain some insight by considering the pinning for the regular domain pattern with a period $2L$ as L increases.

When L is small, a single one-dimensional (1D) vortex chain with the vortex-vortex separation a is pinned by each domain. The average area per vortex is $aL=\Phi_0/2H$. Shown in Fig. 4(c) is a calculated using the observed values of H_1, H_2, and L. The inset shows vortex-domain configurations at H_1 (red) and H_2 (blue). Interestingly, $a=773$ nm at H_1 is identical to that of the Abrikosov lattice constant in continuous film, $a^2=(4/3)^{1/2}\Phi_0/H_1$, suggesting the vortex chains are correlated across neighboring domains to form Abrikosov lattice (red inset). In the large L limit, the vortex chains form Abrikosov lattice *within* each domain with $a^2=(4/3)^{1/2}\Phi_0/2H_3$, from which we obtain $a=364$ nm using $H_3=90$ Oe as shown in Fig. 4(c) by the horizontal line. In between is the transition region exemplified by $\theta=15°$, where H_3 peak appears along with H_2, sharing the same H_3 for $\theta>15°$. This signals the formation of double vortex chains inside domains, separated by a distance $h<L$ (green configuration in the inset). The average area per vortex is $bL/2=\Phi_0/2H_3$, where b is the separation along each chain and a is defined by $a^2=(b/2)^2+h^2$. We estimate h for $\theta=15°$ by noticing that a in the 1D chain at H_2 should be comparable to a in double chain at H_3, which gives $h=0.6L$. Using this value we calculate a for intermediate L. The points calculated with $h=0.6L$ run through the horizontal Abrikosov line.

The distribution of L in the SFB results in variation in the local vortex patterns. However, with the exception for $\theta=15°$, for every other θ there is only one matching field, suggesting that the configurations discussed above are quite robust. The matching conditions consistent with the vortex chains have been observed in the case of Ni wires on Nb films.[21] Recently, a direct imaging by the scanning tunneling microscopy has revealed the formation of multiple vortex chains in $NbSe_2$ with Py on the top.[9]

As shown in Fig. 4(a), with increasing θ, the suppression of U_0 at $H \leq 40$ Oe increases. This is due to the local stray field as shown in Fig. 1(b). At the center of the domain, the stray field scales as $1/L$, hence U_0 at $H \approx 1$ Oe follows a similar dependence. In addition, the confinement of vortices by wider domains is less effective; single vortices are free to flow until the vortex density reaches the matching value. This results in the H independent U_0 at $H \leq 40$ Oe for large L.

Finally we mention the finite-T effects. The activation energy U_0 at $T=0$ for the sF state is the lowest as shown in Fig. 4(a). At finite T, $U(T,H)=U_0(H)[1-T/T_c(H)]$ such that at $T=7.882$ K and for $H \leq 50$ Oe, $U(T,H)$ for sF is larger than that for $\theta=90°$ as shown in Fig. 4(d). This accounts for both the suppression of the critical current and the plateau in the resistance observed for $H \leq 50$ Oe.

In conclusion, we have used a unique angle-dependent demagnetization procedure to tune the width of domains in a single planar SFB. This allows us to continually tune the phase boundary from that of a single maximum to the reentrant one. By extracting the activation energy for vortex pinning in the tunable SFB, we have made a comprehensive study of vortex pinning on domain width, temperature, and magnetic field in the structure with randomly oriented stripe domains.

This work was supported by NSF under Grant No. DMR05-20491 and by Polish MNiSW under Grant No. N202 058 32/1202.

[1] I. F. Lyuksyutov and V. L. Pokrovsky, Adv. Phys. **54**, 67 (2005).
[2] A. Yu. Aladyshkin *et al.*, Supercond. Sci. Technol. **22**, 053001 (2009), and references within.
[3] M. Velez *et al.*, J. Magn. Magn. Mater. **320**, 2547 (2008), and references within.
[4] A. I. Buzdin and A. S. Mel'nikov, Phys. Rev. B **67**, 020503(R) (2003); A. Yu. Aladyshkin *et al.*, *ibid.* **68**, 184508 (2003).
[5] Z. Yang *et al.*, Nature Mater. **3**, 793 (2004).
[6] W. Gillijns *et al.*, Phys. Rev. Lett. **95**, 227003 (2005); W. Gillijns *et al.*, Phys. Rev. B **76**, 060503(R) (2007).
[7] A. Yu. Aladyshkin and V. V. Moshchalkov, Phys. Rev. B **74**, 064503 (2006).
[8] V. Vlasko-Vlasov *et al.*, Phys. Rev. B **77**, 134518 (2008); V. K. Vlasko-Vlasov *et al.*, *ibid.*, **78**, 214511 (2008); A. Belkin *et al.*, *ibid.* **77**, 180506(R) (2008).
[9] G. Karapetrov *et al.*, Phys. Rev. B **80**, 180506(R) (2009).
[10] L. N. Bulaevskii *et al.*, Appl. Phys. Lett. **76**, 2594 (2000); Yu. I. Bespyatykh *et al.*, Sov. Phys. Solid State **43**, 1827 (2001).
[11] M. Z. Cieplak *et al.*, J. Appl. Phys. **97**, 026105 (2005); M. Z. Cieplak *et al.*, Phys. Status Solidi C **2**, 1650 (2005).
[12] M. Feigenson, *et al.*, J. Appl. Phys. **97**, 10J120 (2005).
[13] O. Hellwig *et al.*, J. Magn. Magn. Mater. **319**, 13 (2007).
[14] L. Y. Zhu *et al.*, Phys. Rev. Lett. **101**, 017004 (2008).
[15] M. Tinkham, *Introduction to Superconductivity* (Dover, New York, 2004).
[16] T. T. M. Palstra *et al.*, Phys. Rev. B **41**, 6621 (1990).
[17] O. Brunner *et al.*, Phys. Rev. Lett. **67**, 1354 (1991).
[18] J. W. P. Hsu and A. Kapitulnik, Phys. Rev. B **45**, 4819 (1992).
[19] M. Inui *et al.*, Phys. Rev. Lett. **63**, 2421 (1989).
[20] S. Martin and A. F. Hebard, Phys. Rev. B **43**, 6253 (1991).
[21] D. Jaque *et al.*, Appl. Phys. Lett. **81**, 2851 (2002).